





Zinc finger protein 280C contributes to colorectal tumorigenesis by maintaining epigenetic repression at H3K27me3-marked loci

Ying Ying^{a,b}, Maolin Wang^{a,c}, Yongheng Chen^a, Meiqi Li^a, Canjie Ma^a, Junbao Zhang^a, Xiaoyan Huang^a, Min Jia^a, Junhui Zeng^a, Yejun Wang^a, Lili Li^d , Xiaomei Wang^a, Qian Tao^d, and Xing-sheng Shu^{a,b,1} 

Edited by Peter Jones, Van Andel Institute, Grand Rapids, MI; received November 17, 2021; accepted April 1, 2022

Dysregulated epigenetic and transcriptional programming due to abnormalities of transcription factors (TFs) contributes to and sustains the oncogenicity of cancer cells. Here, we unveiled the role of zinc finger protein 280C (ZNF280C), a known DNA damage response protein, as a tumorigenic TF in colorectal cancer (CRC), required for colitis-associated carcinogenesis and *Apc* deficiency-driven intestinal tumorigenesis in mice. Consistently, *ZNF280C* silencing in human CRC cells inhibited proliferation, clonogenicity, migration, xenograft growth, and liver metastasis. As a C2H2 (Cys2-His2) zinc finger-containing TF, ZNF280C occupied genomic intervals with both transcriptionally active and repressive states and coincided with CCCTC-binding factor (CTCF) and cohesin binding. Notably, ZNF280C was crucial for the repression program of trimethylation of histone H3 at lysine 27 (H3K27me3)-marked genes and the maintenance of both focal and broad H3K27me3 levels. Mechanistically, ZNF280C counteracted CTCF/cohesin activities and condensed the chromatin environment at the cis elements of certain tumor suppressor genes marked by H3K27me3, at least partially through recruiting the epigenetic repressor structural maintenance of chromosomes flexible hinge domain-containing 1 (SMCHD1). In clinical relevance, ZNF280C was highly expressed in primary CRCs and distant metastases, and a higher ZNF280C level independently predicted worse prognosis of CRC patients. Thus, our study uncovered a contributor with good prognostic value to CRC pathogenesis and also elucidated the essence of DNA-binding TFs in orchestrating the epigenetic programming of gene regulation.

ZNF280C | transcription factor | epigenetic repression | CTCF | colorectal cancer

As the third-most commonly diagnosed cancer in 2020, colorectal cancer (CRC) remains the second leading cause of global cancer death in adults, accounting for 10.0% of total new cases and 9.4% of total deaths, respectively (1). It is well established that most CRCs develop from a multistep process following the adenoma–carcinoma sequence in which the initial formation of dysplastic adenoma is driven by early genetic and epigenetic alterations, such as *APC* gene mutations and *MLH1* methylation, and the transformation of adenoma to adenocarcinoma is fostered by multiple other genetic defects, such as gain-of-function mutations of the *KRAS* oncogene and inactivating mutations of the tumor suppressor gene *TP53* (2, 3). Among the factors involved in the molecular pathogenesis of CRC, some directly control gene transcription (e.g., *MYC* and *p53*) and others alter transcriptional outputs through various regulatory mechanisms (e.g., *APC/β-catenin* axis) (3, 4). In fact, transcription dysregulation has been considered a fundamental feature of cancer cells, and dependency on key oncogenic transcription regulators confers substantial growth advantages to cancer cells, which has been leveraged for therapeutic intervention in several cancers including CRC (5, 6). Intense efforts in the past decades unveiled multiple components of general transcription machinery and epigenetic regulators as critical players during the tumorigenesis of CRC (7), but the roles of DNA-binding transcription factors (TFs) that determine the site specificity of the regulatory apparatus remain poorly understood.

The C2H2 (Cys2-His2)-type zinc finger (ZnF)-containing proteins represent the largest family of TFs in the human genome, contributing in large part to the diversity of sequence-specific affinity among all known TFs (8, 9). The various functions of C2H2 ZnF TFs have been implicated in development and diseases, including cancer (8, 10). For instance, CTCF (CCCTC-binding factor), an 11 C2H2 ZnF-containing TF, is a key regulator of higher-order genome organization and local cis-elements topology (e.g., promoter–enhancer interaction), thereby fine-tuning transcription activity under different physiological and pathological contexts (11). Misregulation of

Significance

This study uncovered the role of ZNF280C, a known DNA damage response protein, as a tumorigenic transcription regulator that contributes to colorectal tumorigenesis and metastasis through maintaining an epigenetic repression program at key cancer gene loci. These findings identified a contributor with potential prognostic value to colorectal pathogenesis and provide mechanistic insight to the essential function of transcription factor in fine-tuning the activity of chromatin regulators for proper transcription control.

Author affiliations: ^aSchool of Medicine, Health Science Center, Shenzhen University, Shenzhen 518060, China; ^bMarshall Laboratory of Biomedical Engineering, Health Science Center, Shenzhen University, Shenzhen 518060, China; ^cCollege of Pharmacy, Shenzhen Technology University, Shenzhen, 518000, China; and ^dDepartment of Clinical Oncology, State Key Laboratory of Translational Oncology, Sir YK Pao Center for Cancer and Li Ka Shing Institute of Health Sciences, The Chinese University of Hong Kong, Hong Kong 00000, China

Author contributions: X.-s.S. conceived and supervised research; Y.Y., M.W., Y.C., M.L., C.M., J. Zhang, X.H., M.J., J. Zeng, Y.W., L.L., X.W., Q.T., and X.-s.S. performed research; M.W. contributed new reagents/analytic tools; Y.Y., M.W., Y.C., Q.T., and X.-s.S. analyzed data; and Y.Y. and X.-s.S. wrote the paper.

The authors declare no competing interest.

This article is a PNAS Direct Submission.

Copyright © 2022 the Author(s). Published by PNAS. This article is distributed under [Creative Commons Attribution-NonCommercial-NoDerivatives License 4.0 \(CC BY-NC-ND\)](https://creativecommons.org/licenses/by-nc-nd/4.0/).

¹To whom correspondence may be addressed. Email: shu@szu.edu.cn.

This article contains supporting information online at [http://www.pnas.org/lookup/suppl/doi:10.1073/pnas.2120633119/-DCSupplemental](https://www.pnas.org/lookup/suppl/doi:10.1073/pnas.2120633119/-DCSupplemental).

Published May 23, 2022.

CTCF function has been implicated in a broad spectrum of tumors, with the mutations of CTCF-binding sites as the most frequent genetic alteration in the noncoding tumor genome discovered thus far (12–14). In addition to CTCF, several other TFs with C2H2 ZnF domains are involved in maintaining physiological homeostasis of the intestinal epithelium or pathogenesis of CRC, such as KLF4 (15, 16), KLF5 (17, 18), ZEB1 (19), ZNF281 (20, 21), and ZNF746 (22). Nonetheless, the vast majority of C2H2 ZnF TFs are still uncharacterized in CRC and other common cancers. Moreover, previous studies mainly focused on the direct transcription control by individual TFs, while our understanding about how TFs, in concert with other transcription regulators, actively shape the chromatin environment through modulating dynamics of epigenetic states at cis-regulatory elements has just begun to develop.

In this study, we identified zinc finger protein 280C (ZNF280C or ZPET), a protein known to inhibit homologous recombination during DNA damage response (23), as a crucial contributor to colorectal tumorigenesis and further elucidated the mechanism by which ZNF280C regulates CTCF and cohesin activities at trimethylation of histone H3 at lysine 27 (H3K27me3)-marked cis-regulatory elements of key cancer genes.

Results

ZNF280C Is Highly Expressed in Primary CRCs and Distant Metastases and a Higher ZNF280C Level Strongly Predicts Worse Prognosis of Patients. In order to search for genes involved in CRC pathogenesis, we surveyed multiple CRC datasets generated from high-throughput messenger RNA (mRNA) expression profiling technologies and found that *ZNF280C* was dramatically up-regulated in CRC samples when compared to normal colon or rectum controls in all the datasets we examined (Fig. 1*A* and *SI Appendix*, Fig. S1*A* and *B*). *ZNF280C* expression was even elevated in benign colon adenomas compared to matched control samples (Fig. 1*B*). Notably, higher *ZNF280C* expression was associated with worse overall and relapse-free survival of CRC patients (Fig. 1*C* and *SI Appendix*, Fig. S1*C*).

Concordantly, by using tissue microarray technology for an independent cohort of CRC patients, we found that ZNF280C protein expression was higher in primary CRC samples than in adjacent normal colons (Fig. 1*D* and *E*). Moreover, high ZNF280C expression was observed in distant metastases from multiple sites including liver, lung, and ovary (Fig. 1*D*). In line with this finding, the mRNA expression level of *ZNF280C* was higher in CRC patients at M1 stage (with distant metastasis) than those at M0 stage (*SI Appendix*, Fig. S1*D*). Remarkably, a higher ZNF280C protein level strongly predicted poorer overall survival of CRC patients even after controlling for the effect of other classic prognostic factors, such as age, clinical stage, pathologic grade, and lymph node status (Fig. 1*F* and *G*). These results indicate that overexpression of ZNF280C is likely to be an early and common event during the development of CRC, which may be essential for malignant transformation and progression.

As *ZNF280C* was shown to be a candidate cancer gene, we wondered whether it might also play a role in other common cancers in addition to CRC. Strikingly, *ZNF280C* was found to be significantly up-regulated in 12 out of 18 cancer types that we evaluated (*SI Appendix*, Fig. S2*A* and *B*), and its higher expression was associated with the worse prognosis of multiple cancers (*SI Appendix*, Fig. S2*C*), suggesting that ZNF280C may act as a broad oncogene in tumors with diverse tissue of origin.

Zfp280c Is Required for Colitis-Associated Colorectal Carcinogenesis and Apc Deficiency-Driven Intestinal Tumorigenesis in Mice. To investigate the functional contribution of ZNF280C to CRC development, we first created C57BL/6J mice harboring a genetic deletion spanning exon 3 to the end of the *Zfp280c* gene, the mouse homolog of *ZNF280C*, and verified the elimination of *Zfp280c* gene products at both the mRNA and protein levels in these transgenic mice (Fig. 2*A*). We then used the AOM/DSS-induced colitis-associated cancer (CAC) model to evaluate the impact of *Zfp280c* depletion on colorectal tumorigenesis (Fig. 2*B* and *C*). The results showed that *Zfp280c* knock-out greatly alleviated the tumor burden of colon and markedly inhibited the formation of large tumors (≥ 5 mm) (Fig. 2*D–F*). Moreover, knock-out of *Zfp280c* led to a notable decrease in adenomas of high-grade dysplasia (Fig. 2*G*) and a concomitant reduction of Ki-67 positive cells in the colon epithelium (Fig. 2*H* and *I*).

APC mutation is a well-documented driver for CRC, affecting more than 80% of patients with sporadic colorectal tumors, and germline *APC* mutation gives rise to familial adenomatous polyposis, which is highly susceptible to CRC development (24). Therefore, we next explored the oncogenic function of ZNF280C with the *Apc^{min}* mouse model, which harbors a heterozygous truncating mutation at codon 850 of the *Apc* gene and develops adenomas throughout the intestinal tract at an age of 4 to 6 mo spontaneously (25). Remarkably, knock-out of *Zfp280c* in *Apc^{min}* mice significantly prolonged the lifespan of these mice (median survival time of 42.3 wk), when compared to the *Apc^{min}* mice with wild-type *Zfp280c* alleles (median survival time of 24.6 wk; $P < 0.0001$) (Fig. 3*A*). Intriguingly, the female *Apc^{min}* mice with hemizygous *Zfp280c* (located in the X chromosome) deficiency showed a similar pattern (median survival time of 43.6 wk) as the ones without both *Zfp280c* alleles (Fig. 3*A*). Furthermore, *Zfp280c*-null *Apc^{min}* mice developed fewer polyps in both the small intestine and the colon than *Zfp280c*-wild-type *Apc^{min}* mice at the age of 20 to 24 wk (Fig. 3*B* and *C*) and showed a consistent decrease in the tumor burden across the intestinal tract (Fig. 3*D* and *E*). Pathological inspection revealed frequent carcinoma-like high-grade adenomas and a higher level of Ki-67-positive cells in the small intestine and colon of *Zfp280c*-wild-type *Apc^{min}* mice, while in contrast the intestinal epithelium of *Zfp280c*-null *Apc^{min}* mice was largely normal with fewer Ki-67-positive cells (Fig. 3*F* and *G* and *SI Appendix*, Fig. S3*A* and *B*). These findings indicate that *Zfp280c* is required for intestinal carcinogenesis and malignant progression in mice.

Silencing of ZNF280C Impairs the Oncogenic Potential of CRC Cells. We next tested whether ZNF280C also plays an oncogenic role in human CRC cells. Compared to the immortalized colonic epithelial cell line NCM460, ZNF280C was expressed at a higher level in most CRC cell lines that we examined (*SI Appendix*, Fig. S4*A*). *ZNF280C*-targeting short-hairpin RNAs (shRNAs) controlled by the tetracycline-inducible promoter were stably transduced into three CRC cell lines, RKO, HCT116, and SW620, in which *ZNF280C* expression was silenced by treatment with doxycycline (Fig. 4*A*). As a result, induced *ZNF280C* silencing impeded cell proliferation (Fig. 4*B*) and weakened the monolayer (Fig. 4*C* and *SI Appendix*, Fig. S4*B* and *C*) and soft-agar (Fig. 4*D* and *SI Appendix*, Fig. S4*D* and *E*) colony formation ability in these three cell lines. Moreover, induced *ZNF280C* down-regulation impaired the tumor xenograft formation capacity of RKO cells (Fig. 4*E*

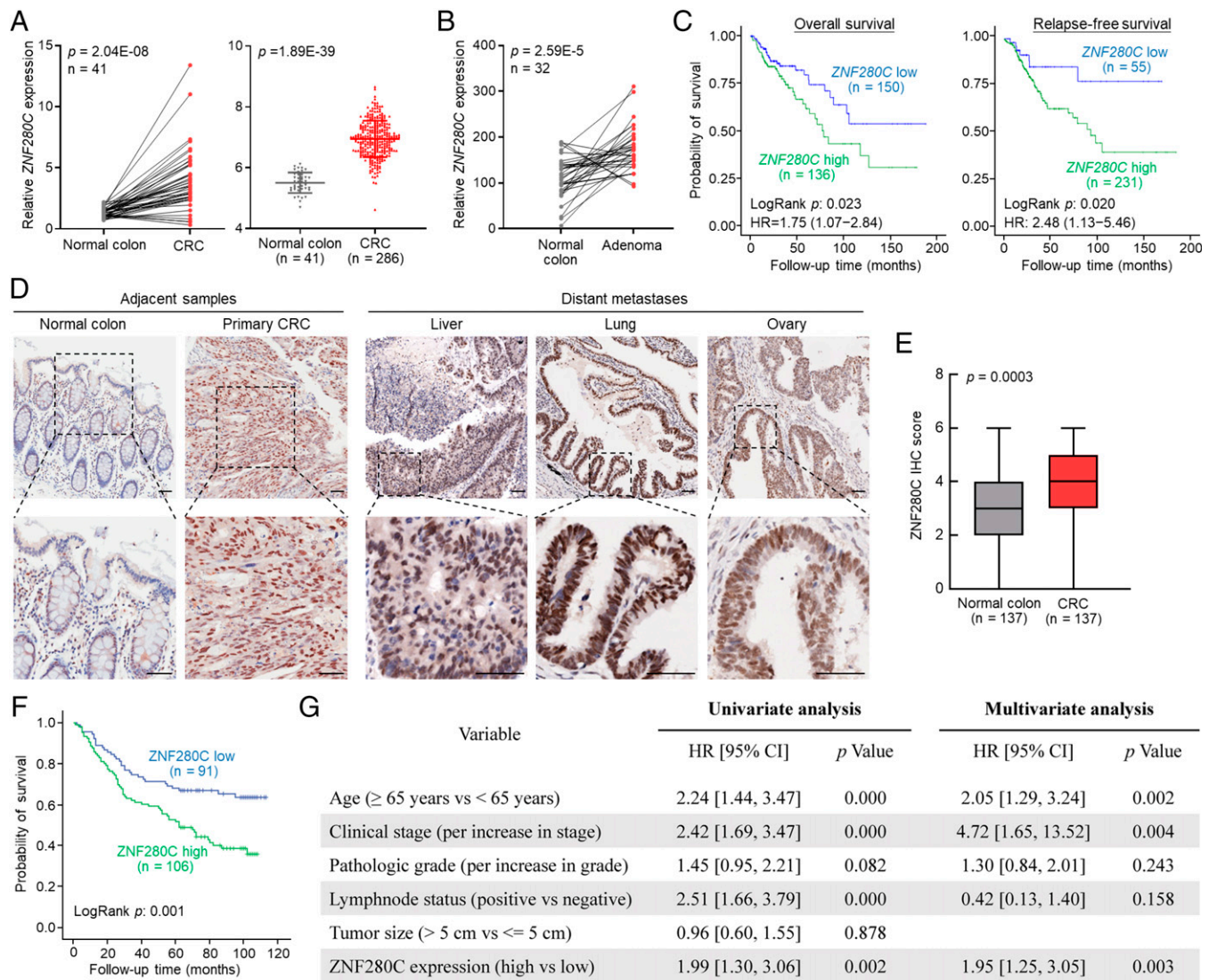


Fig. 1. ZNF280C is highly expressed in primary CRCs and distant metastases, and a higher ZNF280C level strongly predicts worse prognosis of patients. (A) mRNA expression level of *ZNF280C* in normal colon and primary CRC tissues. Data were extracted from the TCGA data portal. (B) Expression of *ZNF280C* in colon adenomas and matched normal tissues. Source data were from GSE8671. (C) Overall and relapse-free survival of TCGA CRC patients categorized by *ZNF280C* expression levels. Statistical significance was determined by the log-rank test. (D) Representative photos of ZNF280C immunohistochemistry (IHC) analysis using tissue microarray. (E) Quantification of the ZNF280C IHC results in matched normal colon and primary CRC tissues. Significance was evaluated by paired *t* test. (F) Overall survival curve of CRC patients categorized by ZNF280C protein levels determined by IHC. (G) Results of univariate and multivariate Cox regression analyses using clinical parameters of CRC patients and ZNF280C protein level as input variables. HR, hazard ratio.

and F), which was further verified by constantly knocking-down *ZNF280C* in the same cells (Fig. 4 G and H).

As *ZNF280C* was highly expressed in both primary tumors and metastases of CRC patients, we then sought to determine whether it is involved in the dissemination of CRC cells. Indeed, the silencing of *ZNF280C* suppressed CRC cell migration in vitro (Fig. 4 I and SI Appendix, Fig. S4 F and G) and liver metastasis in vivo (Fig. 4 J and K). Taking the above data together, we found that *ZNF280C* is required for maintaining the tumorigenic potential of CRC cells, but the mechanism by which *ZNF280C* exerts its oncogenic functions remains undefined.

ZNF280C Occupies Both Transcriptionally Active and Repressive Chromatin Regions and Coincides with CTCF and Cohesin Binding. The physiological and pathological roles of *ZNF280C* mostly remained unclear thus far, with only one study pinpointing its function in repressing homologous recombination during DNA damage repair (23). The *ZNF280C* protein

contains a domain of unknown function in its N terminus, followed by nine C2H2-type ZnF domains across its middle region and C terminus (Fig. 5A). Immunofluorescence staining showed that *ZNF280C* was localized in the cell nucleus with a discrete and focal enrichment pattern (Fig. 5B and SI Appendix, Fig. S5A), and *ZNF280C* down-regulation induced the reversion of multiple transcriptional signatures associated with malignant behaviors of cancer cells, such as proliferation, metastasis, and cell cycle progression (Fig. 5C and SI Appendix, Fig. S5B). To test whether *ZNF280C* acts as a DNA-binding transcription factor in a site-specific manner, we performed chromatin immunoprecipitation sequencing (ChIP-seq) for *ZNF280C* in RKO cells, together with several histone modifications that are commonly used for defining chromatin states. As a result, we detected 1,499 highly confident binding sites for *ZNF280C* across the genome (Fig. 5D). The ChIP-seq signal around these *ZNF280C*-binding sites was significantly decreased upon *ZNF280C* silencing (SI Appendix, Fig. S5C), and the same set of sites was also enriched by *ZNF280C* ChIP-seq in another

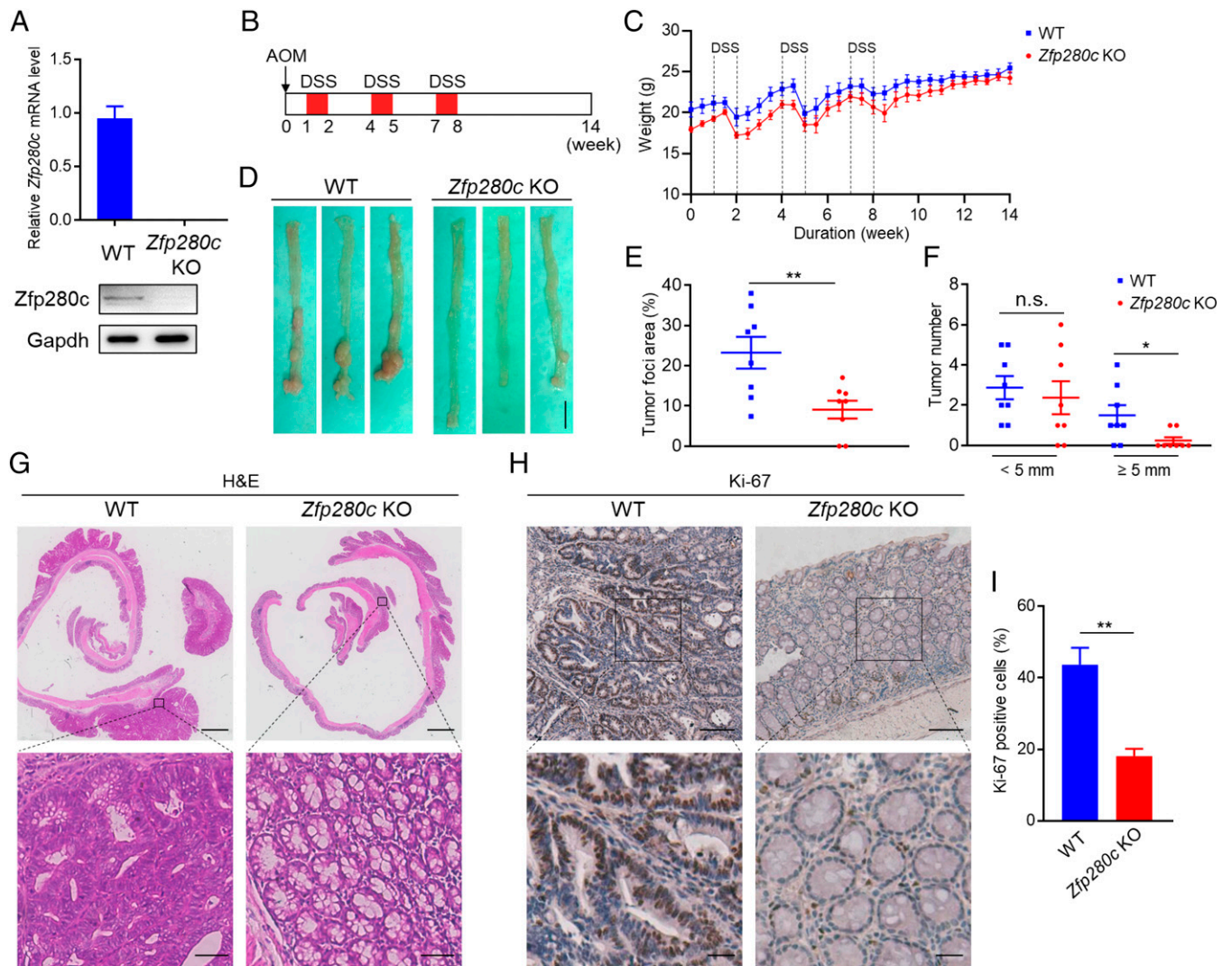


Fig. 2. *Zfp280c* deficiency impedes colitis-associated colorectal carcinogenesis in mice. (A) mRNA and protein expression level of ZNF280C were examined in colon tissues from wild-type or *Zfp280c* knock-out mice. Gapdh was used as an internal control for qPCR and a loading control for Western blot. (B) Diagram showing the experimental procedure of chemical-induced CAC mouse model. (C) Body weight of the mice described in (B) with the genotype indicated. (D) Representative photos of colon dissected from the mice described in (B) (Scale bar, 1 cm). (E) tumor foci area and (F) tumor number of the colon from the mice described in (B). Representative photos of H&E staining (G) and Ki-67 IHC analysis (H, Left) of the colon tissues dissected from the mice described in (B). (H, Right) Quantification of the Ki-67 IHC results. (G) (Scale bars, upper panel of photos, 1,000 μ m; bottom panel, 50 μ m.) (H) (Scale bars, upper panel, 100 μ m; bottom panel, 25 μ m.) KO, knock-out; n.s., not significant; WT, wild-type. * $P < 0.05$; ** $P < 0.01$.

model cell line, K562 (SI Appendix, Fig. S5D), verifying the specificity of the ZNF280C antibody. Interestingly, clustering of the ZNF280C binding sites using their associated chromatin features separated them into two distinct categories: One was strongly correlated with a high level of histone modifications that mark active transcription events, such as trimethylation of histone H3 at lysine 4 (H3K4me3) and acetylation of histone H3 at lysine 27 (H3K27ac) (named as type I), while the other was nearly devoid of these active marks (named as type II) (Fig. 5D). Both types of sites showed deep conservation of the sequences around peak centers (SI Appendix, Fig. S5E). Chromatin state annotation using the ChromHMM method (SI Appendix, Fig. S5F) revealed that type I ZNF280C binding sites were mainly located in active promoters (91.4%) (Fig. 5E). In contrast, type II sites were more frequently found in repressive chromatin regions, such as heterochromatin (39.9%) and H3K27me3-repressed domains (12.4%) (Fig. 5E). In line with this finding, cis-regulatory element annotation based on physical distance to genes located most type I sites at promoter areas (95.9%) while type II sites were more commonly assigned to distal

intergenic regions (44.3%) and gene introns (32.3%) (SI Appendix, Fig. S5G). In accordance, chromatin accessibility analysis showed that type I sites mostly demarcated open chromatin regions, and interestingly, type II sites remained accessible at a limited level within repressive chromatin regions (Fig. 5F and SI Appendix, Fig. S5 H–J), suggesting that ZNF280C might be involved in regulating the transcription of genes with diverse basal activities. In addition, metagene profile analysis further confirmed the enrichment of ZNF280C at the promoter and transcription start site of genes (Fig. 5G).

Motif analysis identified two different prevailing ZNF280C motifs from the two classes of ZNF280C peaks, along with the motifs of several well-known transcription regulators, such as ZNF143 and E2F3 (Fig. 5H). Surprisingly, the motifs of CTCF were found to be significantly enriched in both types of ZNF280C peaks, although the base composition within the CTCF motifs differed slightly between types (Fig. 5H). Consistently, intensive binding of CTCF around the center of ZNF280C peaks was observed, with a stronger preference on type II sites, which was inversely correlated to the levels of

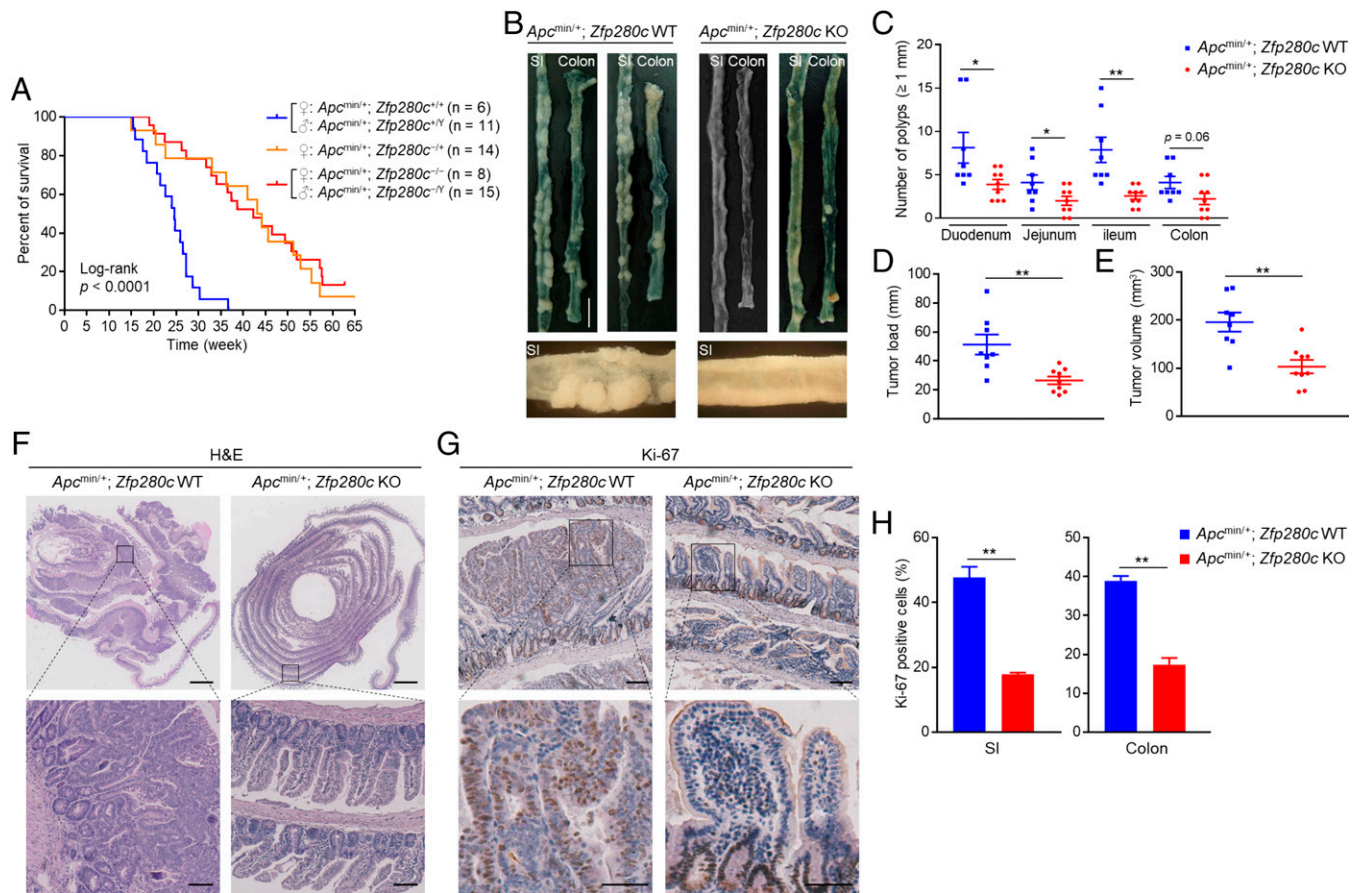


Fig. 3. *Zfp280c* is required for *Apc* deficiency-driven intestinal tumorigenesis in mice. (A) Survival curves of mice with indicated genotypes. Significance was determined by log-rank test. (B) Representative photos of small intestine (ileum) and colon dissected from the mice with indicated genotypes (Scale bar, 1 cm). (C) Number of polyps in the small intestine and colon dissected from the mice with indicated genotypes. (D, E) Tumor load (the sum of the diameter in longer dimension of polyps) and tumor volume (the sum of the volume of polyps) in the small intestine of the mice with indicated genotypes. Representative photos of H&E staining (F) and Ki-67 IHC analysis (G) of the ileum tissues dissected from the mice with indicated genotypes. (F) (Scale bars, upper panel of photos, 1,000 μm ; bottom panel, 100 μm .) (G) (Scale bars, upper panel, 100 μm ; bottom panel, 50 μm .) (H) Quantification of the Ki-67 IHC results in small intestine and colon. KO, knock-out; SI, small intestine; WT, wild-type. * $P < 0.05$; ** $P < 0.01$.

active histone marks (Fig. 5J). Interestingly, RAD21, a core subunit of the cohesin complex that cooperates with CTCF to regulate transcription via functionally organizing the genome architecture (11), showed a highly similar binding pattern over ZNF280C peaks to that of CTCF (Fig. 5J). The site-specific enrichment of ZNF280C in the genome and its sequence context-dependent association with different chromatin features as well as CTCF/cohesin chromatin regulators inspired us to further explore the possibility that ZNF280C controls the transcriptional outputs at certain cancer susceptibility loci through shaping the chromatin environment.

ZNF280C Inactivation Leads to De-Repression of H3K27me3-Marked Genes with Concomitant Decrease of Both Focal and Broad H3K27me3 Levels. In search of transcription modules potentially governed by ZNF280C, we unexpectedly found that multiple sets of H3K27me3-marked genes, including some well-known tumor suppressor genes in CRC (e.g., *CDX2*, *HIC1*, and *EPHB3*) were significantly up-regulated when *ZNF280C* was silenced in human CRC cells or *Zfp280c* was inactivated by genetic knock-out in mice, while in comparison, a random set of repressed genes or genes without H3K27me3 modification largely remained unchanged (Fig. 6A and B). H3K27me3 established by polycomb repressive complex 2 (PRC2) is one of the most abundant histone modifications across the genome and marks the facultative heterochromatin regions and regulatory elements of

numerous genes (26). Therefore, in accordance, the targets of PRC2 were also up-regulated by *ZNF280C* inactivation (Fig. 6A).

In agreement with these findings, we detected a loss of H3K27me3, rather than another repressive histone mark (H2AK119ub) written by PRC1, at both types of ZNF280C binding sites (Fig. 6C and *SI Appendix*, Fig. S6A and B). Consistently, H3K27ac and chromatin accessibility levels of ZNF280C peaks were elevated upon the depletion of *ZNF280C* (Fig. 6C and *SI Appendix*, Fig. S6B and C). Interestingly, the motif of CTCF was dramatically enriched in the assay for transposase-accessible chromatin (ATAC) peaks that emerged after *ZNF280C* silencing (*SI Appendix*, Fig. S6D), implying a role of CTCF in the de-repression of the genes within these regions. Despite focal enrichment at certain cis-regulatory elements, H3K27me3 more commonly marks large genomic spans that are referred to as broad H3K27me3 domains. Remarkably, *ZNF280C* silencing induced a decrease of the H3K27me3 level but not the H2AK119ub level across these H3K27me3 domains, with the active mark H3K27ac remaining stable at a low level (Fig. 6D and *SI Appendix*, Fig. S6E–G). In addition, as expected, type II ZNF280C sites were more frequently located in H3K27me3 domains than in type I sites (*SI Appendix*, Fig. S6H), indicating the context-dependent regulation of H3K27me3-marked genes by ZNF280C. In line with the global reduction of the H3K27me3 level across H3K27me3 domains, a moderate decrease of the H3K27me3

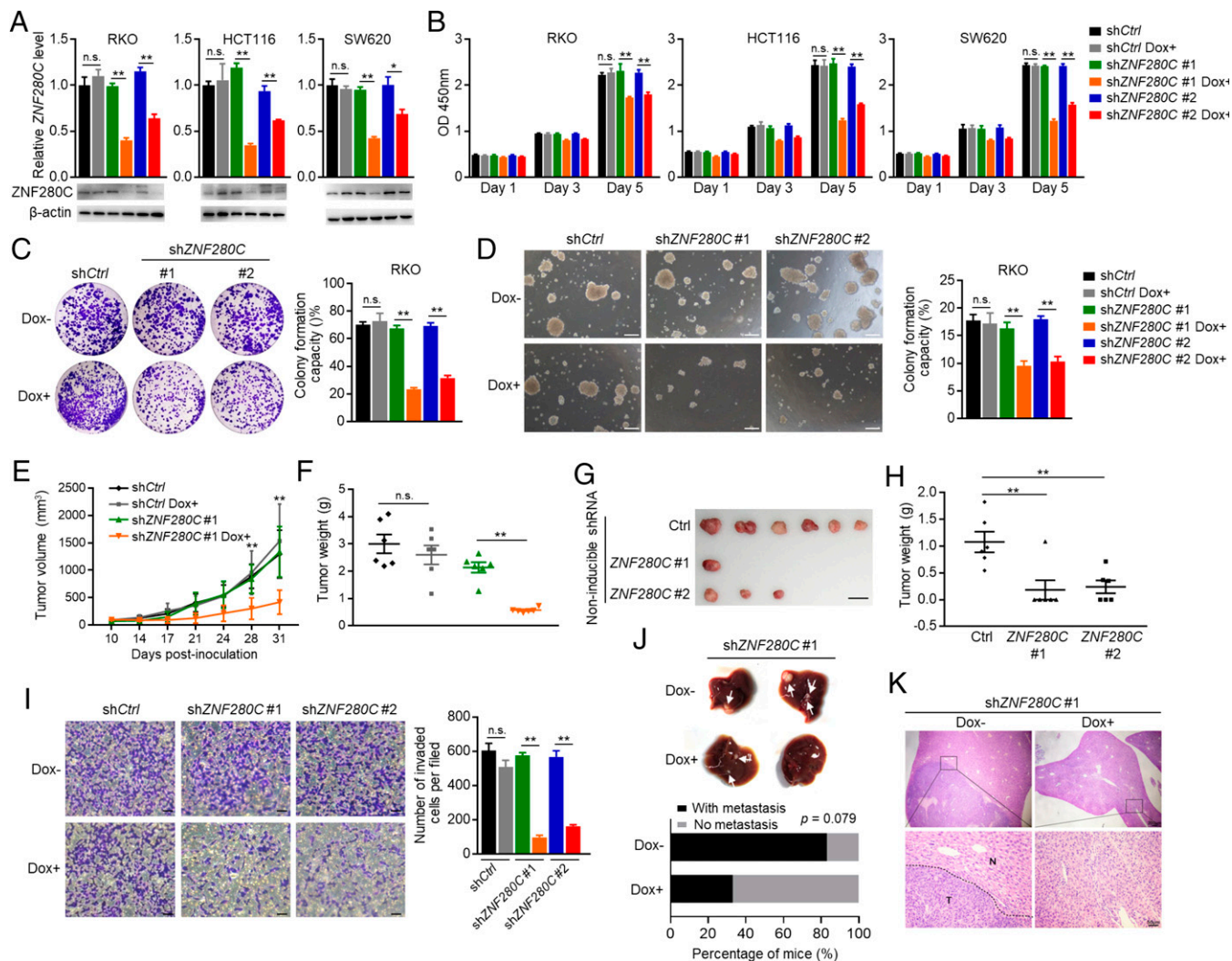


Fig. 4. Silencing of *ZNF280C* impairs the oncogenic potential of CRC cells. (A) RKO, HCT116, and SW620 cells stably transduced with tetracycline-inducible shRNA targeting *ZNF280C* (sh*ZNF280C*#1, #2) or a scramble sequence (sh*Ctrl*) were treated with or without 1 μ M doxycycline (dox) for 72 h, and the resulting cells were subjected to qPCR and Western blot analysis to determine *ZNF280C* levels. β -actin was used as a loading control. (B) Cell proliferation assay using CCK8 for the cells described in (A) at indicated time points. Monolayer (C) and soft-agar (D) colony formation assays using the RKO cells described in (A) (Scale bars, 200 μ m). Tumor xenograft growth curves (E) and tumor weight (F) of the nude mice inoculated with the RKO cells described in (A). (G) RKO cells stably expressing noninducible shRNA targeting a scramble sequence or *ZNF280C* were injected into the flanks of nude mice to allow for growth. The tumors were dissected and photographed 3 wk post inoculation (Scale bar, 2 cm). (H) Weight of the tumors described in (G). (I) Transwell migration assay using the RKO cells described in (A) (Scale bars, 500 μ m). (J) Representative photos of livers from the mice with indicated RKO cells injected to the spleen and statistics of the mice with or without liver metastasis. White arrows indicate sites of liver metastases. *P* value was determined by χ^2 test (*n* = 6 for each group). (K) Representative photos of H&E staining of the liver tissues described in (J) (Scale bar, upper panel of photos, 200 μ m; bottom panel of photos, 50 μ m). The dashed black line indicates the boundary of a metastasis in the liver. N, normal liver tissue; n.s., nonsignificant; T, tumor tissue from a metastasis. **P* < 0.05; ***P* < 0.01.

protein level after *ZNF280C* down-regulation was also observed (SI Appendix, Fig. S6I), further highlighting the crucial role of *ZNF280C* in maintaining the stability of this histone modification.

ZNF280C Cooperates with Structural Maintenance of Chromosomes Flexible Hinge Domain-Containing 1 for H3K27me3 Maintenance by Counteracting CTCF/Cohe sin Activities. To elucidate the role of CTCF and cohesin in transcription events regulated by *ZNF280C*, we first analyzed the occupancy of these two proteins over *ZNF280C* binding sites. The results showed that a substantial part of *ZNF280C* binding sites (15.8% of type I; 49.2% of type II) was occupied by CTCF and RAD21 simultaneously (Fig. 6E). Remarkably, the silencing of *ZNF280C* led to increased CTCF and RAD21 activities at both types of *ZNF280C* binding sites (Fig. 6F and SI Appendix, Fig. S6B), and the increase of CTCF and RAD21 activities upon *ZNF280C* depletion was accompanied by the down-regulation of the H3K27me3 level and elevated

chromatin accessibility at the promoters of certain tumor suppressor genes, such as *EPHB3* and *TP53* (Fig. 6G and SI Appendix, Fig. S6J). In addition, the genome-wide occupancy of *ZNF280C* was highly correlated to that of both CTCF and RAD21 (SI Appendix, Fig. S7A), implying a global functional connection between them. In agreement with our findings, previous studies found that CTCF-binding sites are devoid of H3K27me3 and often mark the boundaries of H3K27me3 domains (27, 28), CTCF has been reported to actively erase the H3K27me3 mark (29), and the depletion of CTCF causes the incorporation of H3K27me3 at cis-regulatory elements of genes (30), as exemplified by the cases of *TP53* (31) and the *HOXA* cluster locus (32).

To further explore how *ZNF280C* maintains H3K27me3 and counteracts CTCF/cohesin activities, we used mass spectrometry to identify proteins co-immunoprecipitated with *ZNF280C* in colon cancer cells. As a result, structural maintenance of chromosomes flexible hinge domain-containing 1

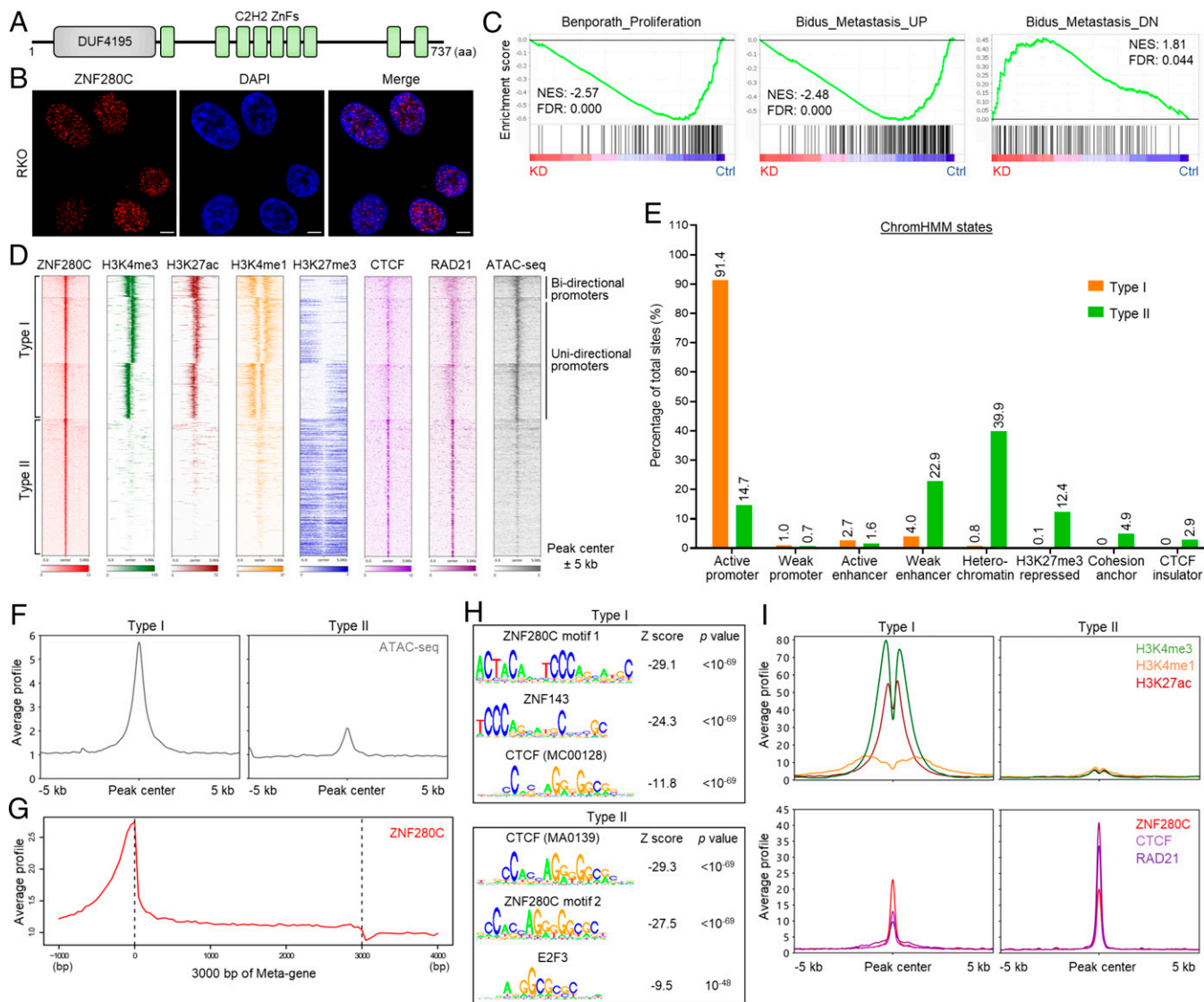


Fig. 5. ZNF280C occupies both transcriptionally active and repressive chromatin regions and coincides with CTCF and cohesin binding. (A) Diagram showing the conserved domains in ZNF280C protein. aa, amino acid; ZnF, zinc finger. (B) Representative images of immunofluorescence showing the nucleus localization of ZNF280C in RKO cells (Scale bars, 5 μ m). (C) RKO cells stably transduced with a tetracycline-inducible shRNA targeting ZNF280C (#1) were treated with (KD) or without (Ctrl) 1 μ g/mL doxycycline (dox) for 72 h and were subject to transcriptome analysis. The differential expression results were then used for GSEA with indicated gene sets. NES, normalized enrichment score; UP, upregulated, DN, downregulated. (D) Heatmaps of the ChIP-seq signal of indicated antibodies as well as signal of ATAC-seq in RKO cells within a 10 kb window around ZNF280C peaks. (E) Annotation of ZNF280C binding sites by the ChromHMM method. (F) Signal profile of ATAC-seq within a 10 kb window around two types of ZNF280C binding sites. (G) Distribution of ZNF280C ChIP-seq profile over metagenes normalized to a length of 3,000 bp. (H) Motifs discovered from two types of ZNF280C peaks. A smaller Z score indicates stronger enrichment of the motif. (I) Signal profile of ChIP-seq with indicated antibodies within a 10 kb window around two types of ZNF280C binding sites.

(SMCHD1) was identified as one of the few proteins that most frequently precipitated with ZNF280C, together with the components of several transcription repressor complexes, such as CHD4, CHD3, DNMT1, and HP1BP3 (Fig. 7A). The interaction between ZNF280C and SMCHD1 was validated by co-immunoprecipitation assays (Fig. 7B and *SI Appendix, Fig. S7B*). In line with this finding, genomic loading of SMCHD1 was enriched at ZNF280C binding sites (Fig. 7C) and partially disturbed by ZNF280C silencing (Fig. 7D). As a noncanonical member of the SMC family proteins, SMCHD1 functions as an epigenetic regulator that is critical for X-chromosome inactivation (33), gene imprinting (34), and Xi compartmentalization (35). SMCHD1-mediated transcriptional repression is mainly achieved by establishing or maintaining DNA CpG methylation and repressive histone modifications, such as H3K27me3, at cis-regulatory elements (36–40). Notably, the genome-wide occupancy of SMCHD1 partially coincides with

that of CTCF, and functional antagonism between SMCHD1 and CTCF has been reported (41), in which Ctf binding was enhanced upon *Smchd1* inactivation and the effect of gene activation by *Smchd1* knock-out was compromised by concurrent *Ctf* depletion. In concert with these findings, we found that the CTCF motif, together with the motif of the transcription repressor Rest, was significantly enriched in SMCHD1 peaks in CRC cells (Fig. 7E). Moreover, the global occupancy of SMCHD1 was strongly correlated with the repressive marks H3K27me3 and H2AK119ub rather than the active marks H3K27ac and H3K4me3 and largely resembled the genomic distribution pattern of CTCF, RAD21, and ZNF280C (Fig. 7F and *SI Appendix, Fig. S7C*). Notably, a substantial part of SMCHD1 binding sites (23%) was colocalized with those of CTCF (Fig. 7G), and the silencing of ZNF280C significantly intervened in the loading of SMCHD1 at these sites (Fig. 7I and J), suggesting that the functional antagonism of ZNF280C

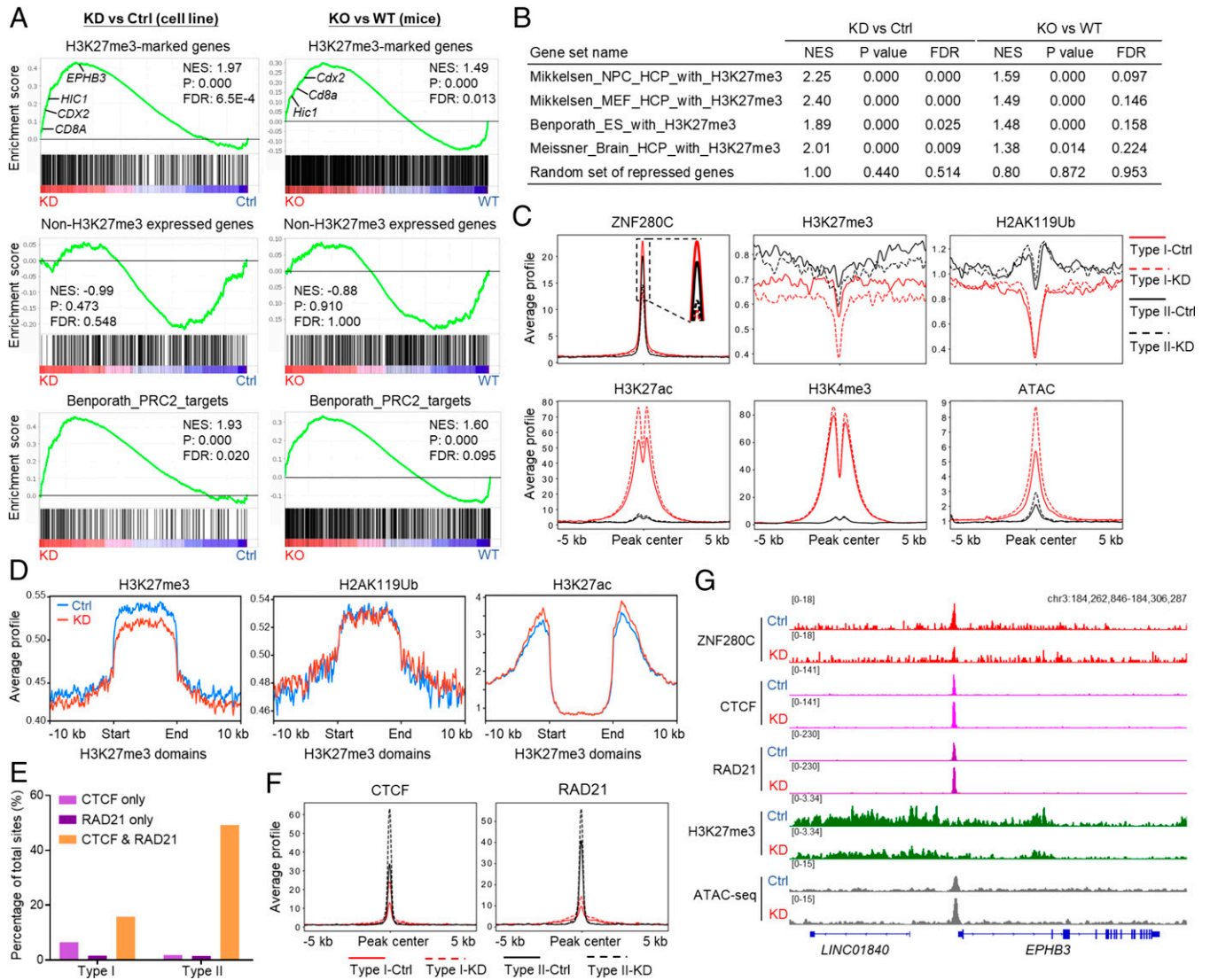


Fig. 6. *ZNF280C* inactivation leads to de-repression of H3K27me3-marked genes with concomitant decrease of both focal and broad H3K27me3 levels. (A, B) GSEA results of indicated gene sets using differential gene expression data after inducible silencing of *ZNF280C* in RKO cells (Left) or depletion of *Zfp280c* in mice (Right). Ctrl, control; KD, *ZNF280C* knock-down; KO, *Zfp280c* knock-out; NES, normalized enrichment score; WT, wild-type; NPC, neural progenitor cells; HCP, high-CpG-density promoters; MEF, mouse embryonic fibroblasts; ES, embryonic stem. (C) Signal profile of ChIP-seq with indicated antibodies or ATAC-seq in RKO cells with or without *ZNF280C* silencing within a 10 kb window around *ZNF280C* binding sites. (D) Signal profile of ChIP-seq with indicated antibodies across the meta-H3K27me3 domains normalized to a length of 10 kb. (E) Fraction of *ZNF280C* binding sites occupied by CTCF or RAD21. (F) Signal profile of ChIP-seq with CTCF or RAD21 antibodies in RKO cells with or without *ZNF280C* silencing within a 10 kb window around *ZNF280C* binding sites. (G) IGV view of ChIP-seq profiles of indicated antibodies and ATAC-seq profiles across the specified genomic regions.

against CTCF/cohesin is at least partially mediated by the epigenetic repressor SMCHD1.

Taken together, we uncovered *ZNF280C* as a contributor to colorectal tumorigenesis and metastasis, comprehensively characterized the chromatin features at *ZNF280C* binding sites, and delineated the functional antagonism between *ZNF280C* and CTCF/cohesin at H3K27me3-marked tumor suppressor loci, which is at least partially mediated by the epigenetic regulator SMCHD1 (Fig. 7K).

Discussion

Transcriptional dependency conferred by the dysregulation of oncogenic transcription factors represents a key feature of cancer cells (5). Here, we report on the role of *ZNF280C*, a ZnF-containing transcription regulator, in CRC pathogenesis. *ZNF280C* belongs to a family of four ZnF proteins (*ZNF280A* to D) sharing high-sequence homology, although the

composition of the carboxyl terminus containing the last two C2H2-type ZnF proteins varies among them. *ZNF280A* (42, 43) and *ZNF280B* (44, 45) have been reported to play tumorigenic roles in cancer, mainly through controlling the transcription of their downstream target genes, while whether *ZNF280C* and *ZNF280D* are involved in tumorigenesis has been unknown. In this study, *ZNF280C* was shown to be a functional cancer gene up-regulated in CRC tissues, but the underlying mechanism for its aberrant activation remains unclear. The *ZNF280C* gene was mutated at a relatively low rate (1 to 3%) in six different CRC genome datasets when compared to some classic cancer genes (SI Appendix, Fig. S8A), and its copy number amplification was also rarely detected (SI Appendix, Fig. S8B). Interestingly, we found that there was a typical CpG island within the promoter of the *ZNF280C* gene (SI Appendix, Fig. S8C) and that the methylation level of its promoter was significantly lower in primary CRC than in adjacent normal colon tissues (SI Appendix, Fig. S8D), suggesting

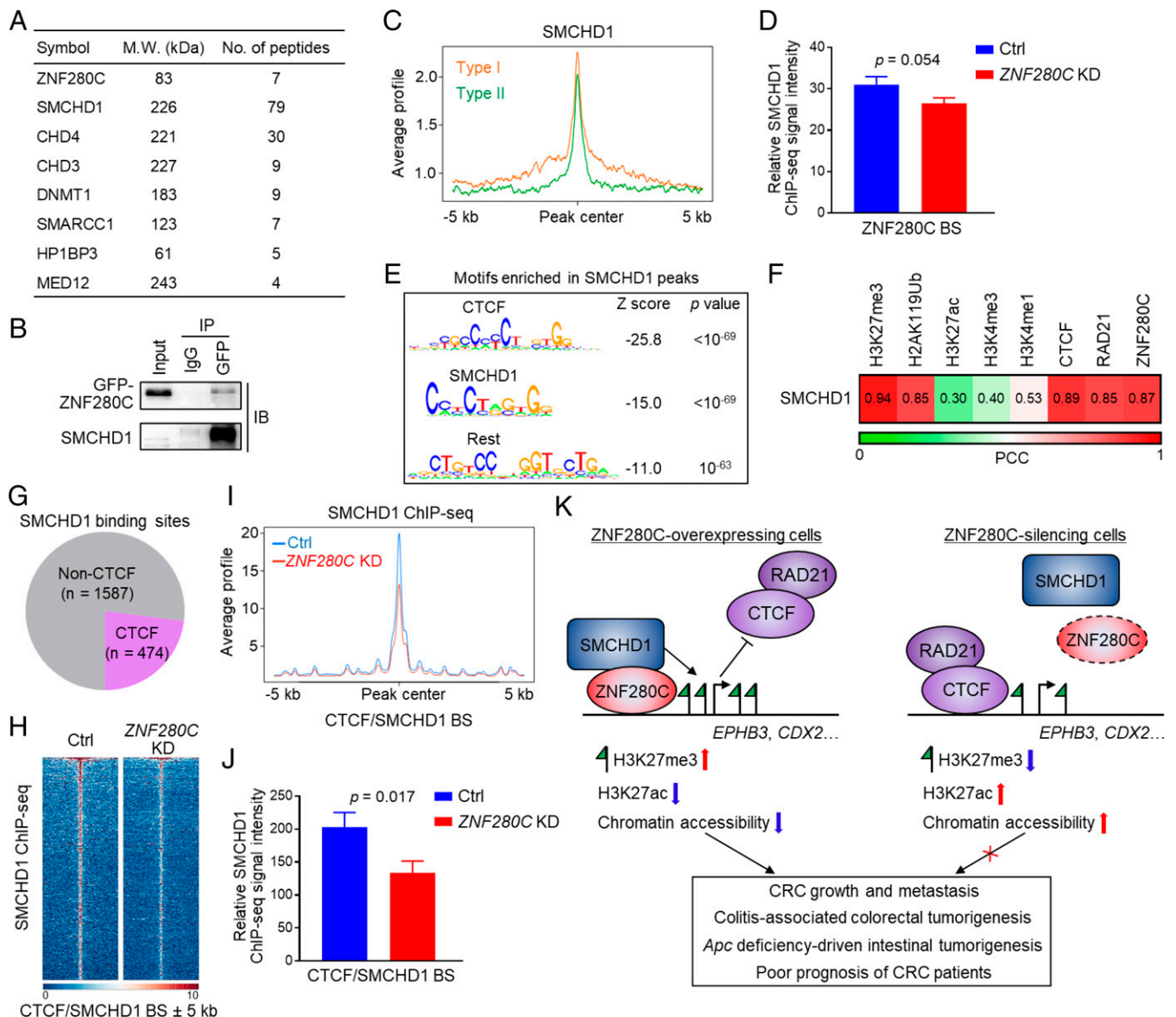


Fig. 7. ZNF280C cooperates with SMCHD1 for H3K27me3 maintenance by counteracting CTCF/cohesin activities. (A) Proteins identified from liquid chromatography–mass spectrometry analysis of immunoprecipitates pulled down by a ZNF280C antibody in RKO cells. (B) Coimmunoprecipitation assay in RKO cells transfected with GFP-ZNF280C plasmid using GFP antibody. IB, immunoblotting; IP, immunoprecipitation. (C) Signal profile of SMCHD1 ChIP-seq in RKO cells within a 10 kb window around ZNF280C binding sites. (D) Quantification of the ChIP-seq signal of SMCHD1 from indicated samples within a 200 bp window (RPGC in a bin size of 10 bp) around the center of ZNF280C binding sites (BS). (E) Motifs enriched in SMCHD1 ChIP-seq peaks. A smaller Z score indicates stronger enrichment of the motif. (F) Heatmap showing the coefficient of the correlations between genome-wide ChIP-seq signal of SMCHD1 and 8 other indicated antibodies (at a resolution of 10 kb) in RKO cells. (G) Pie chart demonstrating the fraction of SMCHD1 binding sites occupied by CTCF (in purple). (H) Heatmaps (H) and signal profile curves (I) showing the difference of SMCHD1 ChIP-seq signal around CTCF/SMCHD1 binding sites (BS) in indicated samples. (J) Quantification of the ChIP-seq signal of SMCHD1 from indicated samples within a 200 bp window (RPGC in a bin size of 10 bp) around the center of CTCF/SMCHD1 binding sites (BS). (K) Diagram illustrating how ZNF280C maintains epigenetic repression at tumor suppressor loci through orchestrating the activities of chromatin regulators including SMCHD1 and CTCF/cohesin, driving the onset and progression of intestinal cancer.

that epigenetic abnormality may be responsible for *ZNF280C* activation in CRC.

Maintaining proper dynamics of H3K27me3 across the genome is crucial for developmental and physiological processes, which often go awry during tumorigenesis (26). In mammalian cells, the balanced activities of the PRC2 and lysine demethylase 6A/B (KDM6A/B) determine the abundance of H3K27me3, but the mechanisms by which the site-specific H3K27me3 pattern is established and maintained are still poorly understood. In this study, we uncovered a crucial role of ZNF280C in maintaining the H3K27me3 level at genomic intervals with enrichment of both ZNF280C and CTCF binding. ZNF280C counteracts the activities of CTCF and cohesin at these sites by recruiting the transcription repressor SMCHD1, which preserves DNA CpG methylation and/

or repressive histone marks including H3K27me3, thereby attenuating the local accessibility to CTCF binding and blocking a CTCF/cohesin-mediated promoter–enhancer interaction that ultimately leads to gene silencing. The writing of H3K27me3 in the genome is largely dependent on the histone methyltransferase activity of a multisubunit complex, PRC2 (26). Considering the crucial role of ZNF280C in H3K27me3 maintenance, it is of interest to explore ZNF280C's functional connection to PRC2 in CRC. Intriguingly, in a gene coexpression analysis of *ZNF280C* in CRC, we unexpectedly found that the mRNA level of *ZNF280C* was strongly correlated to the levels of three PRC2 core subunits, *EZH2*, *EED*, and *SUZ12*, while in contrast it showed no correlation to *RING1A*, a core subunit of the PRC1 complex (SI Appendix, Fig. S9 A and B). This finding suggests that ZNF280C and the key components of

the PRC2 complex are likely to reside in the same transcription regulatory network. However, whether there is transcriptional codependency between ZNF280C and PRC2 and whether they lie in the same oncogenic transcriptional circuitry governed by certain upstream master TFs still await to be further investigated.

Apart from its role in transcription regulation, ZNF280C has been reported to be localized to DNA damage sites, restrict end resection, and repress homologous recombination (HR) (23). The transient repression of transcription and the formation of the condensed chromatin state around DNA break sites ensures the accuracy and efficiency of the repair process (46). Intriguingly, our finding that ZNF280C is critical for maintaining epigenetic repression at H3K27me₃-marked sites raised the possibility that recruitment of ZNF280C to DNA damage sites reshapes the proximal chromatin structure through epigenetic reprogramming to inhibit local transcription and prevents the loading of the MRE11-RAD50-NBS1 complex for end resection. In addition, the inhibitory role of ZNF280C on HR repair might be explained, at least in part, by its functional antagonism against CTCF, which was found to facilitate DNA repair by enhancing HR (47, 48). Therefore, it is of great interest to establish the possible mechanistic link between ZNF280C-mediated epigenetic/transcriptional regulation and its function in DNA damage repair in the future.

To conclude, we unveiled the crucial role of the DNA-binding transcription regulator ZNF280C in CRC pathogenesis and further elucidated its functional antagonism against another key chromatin regulator, CTCF, in maintaining epigenetic repression at certain tumor suppressor loci, illustrating the vulnerability of transcriptional dependency on context-specific TFs that can be potentially targeted for therapeutic intervention in intestinal cancers.

Materials and Methods

Mouse Experiments. *Zfp280c*-deficient C57BL/6J mice were generated by the CRISPR/Cas9-based gene deletion strategy, in which the genomic fragment spanning exons 3 to 19 of the *Zfp280c* gene (Mouse Genome Informatics or MGI: 2387585) was deleted, resulting in the depletion of the *Zfp280c* transcript and protein product. The sequences of the guide RNAs used are listed in *SI Appendix, Table S1*. The *Apc^{min}* mice harboring a heterozygous truncating mutation at codon 850 of the *Apc* gene (MGI: 88039) were obtained from the Jackson Laboratory and were bred to *Zfp280c*-deficient mice for generating *Apc^{min}* mice with *Zfp280c* depletion. All mice were maintained under pathogen-free conditions and fed by a standard chow diet.

For the chemical-induced colitis-associated cancer model, sex-matched mice aged 6 to 8 wk with indicated genotypes were treated with a single intraperitoneal injection of 10 mg/kg AOM (Sigma-A5486). At 7 d post injection, mice were given drinking water containing 2% DSS (MP Biomedical-160110) for 1 wk, and regular water was given over the next 2 wk. After that, another two cycles of DSS treatment were administered following the same procedures. At 14 wk after the AOM treatment, mice were killed, the colon was dissected, the tumor number and dimensions were recorded, and the tissues were kept in 4% paraformaldehyde for histological analysis by hematoxylin and eosin (H&E) staining.

For the tumor xenograft model, RKO cells stably expressing tetracycline-inducible shRNAs targeting *ZNF280C* or a scramble sequence were subcutaneously inoculated to the right flank of female BALB/c nude mice (4×10^6 cells per mouse; 6 mice for each group). The mice were given drinking water containing 2 mg/mL doxycycline (Sigma-D9891) and 5% sucrose or water with 5% sucrose only. One week later, tumor dimensions were measured by vernier caliper every 3 d. Tumor volume was calculated using the following formula: $L \times W^2 \times 0.52$, where L represents the length and W represents the width. For metastasis experiments, the same RKO cells (2×10^6 cells per mouse) as described above were injected into the spleens of nude mice ($n = 6$ per group) and 2 mg/mL doxycycline was administered via drinking water with 5% sucrose from the day after cell inoculation. Six

weeks later, mice were killed and metastases in the liver were imaged. The livers were then fixed in 4% paraformaldehyde, embedded with paraffin, and subject to histological analysis. Mice were allocated to each group randomly by random numbering. All mouse experiments were not conducted in blind.

Mouse handling and experimental procedures in this study were approved (No. AEWC-2019006) by the Animal Ethical and Welfare Committee of Shenzhen University.

ChIP-seq. ChIP experiments were performed as described (49). For detailed procedures of ChIP, please refer to the *SI Appendix, Materials and Methods*. Antibodies used for ChIP are listed in *SI Appendix, Table S2*. Libraries of purified ChIP DNA or input DNA were prepared with the TruSeq DNA Sample Preparation version 2 kit (Illumina) according to the manufacturer's instructions and were sequenced on a HiSeq X Ten platform (Illumina).

For analysis of ChIP-seq data, raw reads were aligned to reference genome hg19 by Bowtie2 (version 2.2.9). The number of total and aligned reads obtained for each sample is listed in *SI Appendix, Table S3*. Peak calling from alignment results was performed using MACS2 (version 2.1.6) using default parameters with a significance level at a q value < 0.05 . No lambda, no model, and broad peak were used for H3K27me₃ samples. The input was used as reference background for peak calling. Blacklist regions from the ENCODE project were filtered out. Motif discovery was performed using the SeqPos motif tool (version 1.0.0) of the Cistrome analysis pipeline (50). The bedGraph files generated from MACS2 were converted to bigwig files using the ucsc bedGraphToBigWig tool. The Integrative Genomics Viewer (IGV) was used to visualize signal profiles and peaks of indicated genomic intervals.

The ChromHMM method (51) was employed to annotate the chromatin state of genomic intervals with the ChIP-seq signal of H3K4me₃, H3K27ac, H3K4me₁, H3K27me₃, CTCF, and RAD21 as inputs. The assignment of functional genomic elements to grouped chromatin states mainly followed the principle reported in the original study (51).

For broad H3K27me₃ domain identification, an algorithm based on a hidden Markov model that was developed recently was used with default parameters (52). For a ChIP signal heatmap and profile curve in given genomic intervals, a score matrix was first calculated using computeMatrix in deeptools (version 3.1.3) at a bin size of 10 bp, then plotHeatmap and plotProfiles in deeptools were used for visualization.

ATAC Sequencing. ATAC sequencing (ATAC-seq) was carried out according to the manufacturer's instructions (Active Motif- 53150). Briefly, the nuclei of 100,000 cells were incubated with the tagmentation master mix containing Tn5 transposase at 37 °C for 30 min. DNA was purified and amplified by PCR, and the library was subject to quality analysis on an Agilent 2100 Bioanalyzer. The qualified library was sequenced on a HiSeq X Ten platform (Illumina). Approximately 130 to 140 million clean reads were acquired for each sample. Alignment of the paired-end reads to the hg19 reference genome was performed using Bowtie2 (version 2.2.9). Genrich (version 0.6) was used for peak calling of ATAC-seq samples. Generation of the bigwig file and profiling of the ATAC-seq signal at given genomic regions was performed using the same procedure as ChIP-seq.

RNA Sequencing and Gene Set Enrichment Analysis. RNA sequencing (RNA-seq) was conducted as reported earlier elsewhere (53). Total RNA was extracted, and mRNA was enriched for library construction. The qualified library was sequenced on the MGISEQ-2000 platform (Beijing Genomics Institute). Raw reads were cleaned using SOAPnuke (version 1.4.1), generating approximately 21 million clean reads per sample. Hisat (version 0.1.6) and Bowtie2 (version 2.3.5) were used to align the clean data to the reference genome (hg19) and reference gene, respectively. Transcript abundance was quantified using HTseq (version 0.11.2), and differentially expressed genes were identified using the edgeR package from the R software.

Gene set enrichment analysis (GSEA) of the RNA-seq data was conducted with the preranked method as previously described (54). All genes differentially expressed between two samples were ranked according to the absolute value of Log₁₀ (false discovery rate [FDR]) with the sign of fold change. The preranked gene list was then loaded for analysis. The number of permutations was set to 1,000 as the default. Gene sets analyzed in this study were from the Molecular Signatures Database except for three gene sets (H3K27me₃-marked genes, non-H3K27me₃-expressed genes, and random set of repressed genes) that were reported elsewhere (55).

Proliferation, Colony Formation, and Transwell Assays. For proliferation assay, cells were seeded in 96-well plates (6,000 to 8,000 cells per well). The Cell Counting Kit-8 (CCK8, Dojindo) reagent was added to the cell culture at the indicated time points, and absorbance at 450 nm was measured after 1 h incubation. For the monolayer colony formation assay, cells were seeded in 6-well plates (500 cells per well) and allowed to grow for 2 wk. Medium and doxycycline were refreshed every 2 d. At the end of the experiment, colonies were stained by crystal violet. For the soft-agar colony formation assay, cells were suspended in growth medium containing 0.35% agar in 24-well plates. Surviving colonies were photographed and counted after approximately 2 to 3 wk. For the migration assay, cells in serum-free medium were seeded in the upper chamber of a transwell insert (Corning) in 24-well plates with medium containing 10% fetal bovine serum in the bottom chamber. After 30 h incubation, migrated cells at the bottom side of the insert membrane were stained with crystal violet. At least five random fields were photographed and counted using a phase-contrast inverted microscope.

Immunoprecipitation, Western Blot, and Liquid Chromatography–Mass Spectrometry. Immunoprecipitation and Western blot were conducted as reported previously (56). For liquid chromatography–mass spectrometry, a digested peptides mixture was first separated by a high-performance liquid chromatography

system (UltiMate3000, Thermo Scientific) and then subjected to tandem mass spectrometry on the Q Exactive Hybrid Quadrupole-Orbitrap platform (Thermo Scientific). Tandem mass spectrometry results were queried in the Uniprot database by Mascot (version 2.3.0) with the significance threshold set to $P < 0.05$. Antibodies used in this study and their working dilution for each application are listed in *SI Appendix, Table S2*. For more information about the materials and methods, refer to *SI Appendix, Materials and Methods*.

Data Availability. ChIP-seq, ATAC-seq, and RNA-seq data generated in this study have been deposited at the Gene Expression Omnibus (GEO) under accession number GSE181856 (<https://www.ncbi.nlm.nih.gov/geo/query/acc.cgi?acc=GSE181856>). Datasets from The Cancer Genome Atlas (TCGA data portal) (57) or GEO database (GSE39582 and GSE8671) (58, 59) are publicly available.

ACKNOWLEDGMENTS. This work was supported by the National Natural Science Foundation of China (82072661, 82070978), the Natural Science Foundation of Guangdong Province (2020A1515010125, 2021A1515012436), and the Shenzhen Commission of Science and Innovation Programs (JCYJ20190808165003697, JCYJ20190808145211234). We thank the Instrumental Analysis Center of Shenzhen University (Xili Campus) for technical support.

- H. Sung *et al.*, Global cancer statistics 2020: GLOBOCAN estimates of incidence and mortality worldwide for 36 cancers in 185 countries. *CA Cancer J. Clin.* **71**, 209–249 (2021).
- H. Brenner, M. Kloor, C. P. Pox, Colorectal cancer. *Lancet* **383**, 1490–1502 (2014).
- S. D. Markowitz, M. M. Bertagnoli, Molecular origins of cancer: Molecular basis of colorectal cancer. *N. Engl. J. Med.* **361**, 2449–2460 (2009).
- G. Jung, E. Hernández-Illán, L. Moreira, F. Balaguer, A. Goel, Epigenetics of colorectal cancer: Biomarker and therapeutic potential. *Nat. Rev. Gastroenterol. Hepatol.* **17**, 111–130 (2020).
- J. E. Bradner, D. Hnisz, R. A. Young, Transcriptional addiction in cancer. *Cell* **168**, 629–643 (2017).
- J. H. Bushweller, Targeting transcription factors in cancer—From undruggable to reality. *Nat. Rev. Cancer* **19**, 611–624 (2019).
- H. Xu *et al.*, Transcription factors in colorectal cancer: Molecular mechanism and therapeutic implications. *Oncogene* **40**, 1555–1569 (2021).
- S. A. Lambert *et al.*, The human transcription factors. *Cell* **172**, 650–665 (2018).
- S. A. Lambert *et al.*, Similarity regression predicts evolution of transcription factor sequence specificity. *Nat. Genet.* **51**, 981–989 (2019).
- M. Cassandri *et al.*, Zinc-finger proteins in health and disease. *Cell Death Discov.* **3**, 17071 (2017).
- M. Merkschlagner, E. P. Nora, CTCF and cohesin in genome folding and transcriptional gene regulation. *Annu. Rev. Genomics Hum. Genet.* **17**, 17–43 (2016).
- R. Katainen *et al.*, CTCF/cohesin-binding sites are frequently mutated in cancer. *Nat. Genet.* **47**, 818–821 (2015).
- Y. A. Guo *et al.*, Mutation hotspots at CTCF binding sites coupled to chromosomal instability in gastrointestinal cancers. *Nat. Commun.* **9**, 1520 (2018).
- E. M. Liu *et al.*, Identification of cancer drivers at CTCF insulators in 1,962 whole genomes. *Cell Syst.* **8**, 446–455.e8 (2019).
- W. Zhang *et al.*, Novel cross talk of Kruppel-like factor 4 and beta-catenin regulates normal intestinal homeostasis and tumor repression. *Mol. Cell. Biol.* **26**, 2055–2064 (2006).
- W. Zhao *et al.*, Identification of Kruppel-like factor 4 as a potential tumor suppressor gene in colorectal cancer. *Oncogene* **23**, 395–402 (2004).
- M. O. Nandan *et al.*, Kruppel-like factor 5 mediates cellular transformation during oncogenic KRAS-induced intestinal tumorigenesis. *Gastroenterology* **134**, 120–130 (2008).
- X. Zhang *et al.*, Somatic superenhancer duplications and hotspot mutations lead to oncogenic activation of the KLF5 transcription factor. *Cancer Discov.* **8**, 108–125 (2018).
- E. Sánchez-Tilló *et al.*, ZEB1 promotes invasiveness of colorectal carcinoma cells through the opposing regulation of uPA and PAI-1. *Clin. Cancer Res.* **19**, 1071–1082 (2013).
- M. Pierdomenico *et al.*, Transcription factor ZNF281: A novel player in intestinal inflammation and fibrosis. *Front. Immunol.* **9**, 2907 (2018).
- C. J. Qin *et al.*, ZNF281 regulates cell proliferation, migration and invasion in colorectal cancer through Wnt/ β -catenin signaling. *Cell. Physiol. Biochem.* **52**, 1503–1516 (2019).
- J. H. Jung *et al.*, Zinc finger protein 746 promotes colorectal cancer progression via c-Myc stability mediated by glycogen synthase kinase 3 β and F-box and WD repeat domain-containing 7. *Oncogene* **37**, 3715–3728 (2018).
- D. M. Moquin *et al.*, Localized protein biotinylation at DNA damage sites identifies ZPET, a repressor of homologous recombination. *Genes Dev.* **33**, 75–89 (2019).
- L. Zhang, J. W. Shay, Multiple roles of APC and its therapeutic implications in colorectal cancer. *J. Natl. Cancer Inst.* **109**, djw332 (2017).
- A. R. Moser, H. C. Pitot, W. F. Dove, A dominant mutation that predisposes to multiple intestinal neoplasia in the mouse. *Science* **247**, 322–324 (1990).
- A. Piunti, A. Shilatifard, The roles of polycomb repressive complexes in mammalian development and cancer. *Nat. Rev. Mol. Cell Biol.* **22**, 326–345 (2021).
- A. Baski *et al.*, High-resolution profiling of histone methylations in the human genome. *Cell* **129**, 823–837 (2007).
- S. Cuddapah *et al.*, Global analysis of the insulator binding protein CTCF in chromatin barrier regions reveals demarcation of active and repressive domains. *Genome Res.* **19**, 24–32 (2009).
- O. Weth *et al.*, CTCF induces histone variant incorporation, erases the H3K27me3 histone mark and opens chromatin. *Nucleic Acids Res.* **42**, 11941–11951 (2014).
- M. Bartkuhn *et al.*, Active promoters and insulators are marked by the centrosomal protein 190. *EMBO J.* **28**, 877–888 (2009).
- E. Soto-Reyes, F. Recillas-Targa, Epigenetic regulation of the human p53 gene promoter by the CTCF transcription factor in transformed cell lines. *Oncogene* **29**, 2217–2227 (2010).
- Y. J. Kim, K. R. Cecchini, T. H. Kim, Conserved, developmentally regulated mechanism couples chromosomal looping and heterochromatin barrier activity at the homeobox gene A locus. *Proc. Natl. Acad. Sci. U.S.A.* **108**, 7391–7396 (2011).
- M. E. Blewitt *et al.*, SmcHD1, containing a structural-maintenance-of-chromosomes hinge domain, has a critical role in X inactivation. *Nat. Genet.* **40**, 663–669 (2008).
- I. Wanigasuriya *et al.*, SmcHD1 is a maternal effect gene required for genomic imprinting. *eLife* **9**, e55529 (2020).
- C. Y. Wang, T. Jégu, H. P. Chu, H. J. Oh, J. T. Lee, SMCHD1 merges chromosome compartments and assists formation of super-structures on the inactive X. *Cell* **174**, 406–421.e25 (2018).
- Y. Sakakibara *et al.*, Role of SmcHD1 in establishment of epigenetic states required for the maintenance of the X-inactivated state in mice. *Development* **145**, dev166462 (2018).
- Z. Huang *et al.*, The chromosomal protein SMCHD1 regulates DNA methylation and the 2c-like state of embryonic stem cells by antagonizing TET proteins. *Sci. Adv.* **7**, eabb9149 (2021).
- C. Dion *et al.*, SMCHD1 is involved in de novo methylation of the DUX4-encoding D4Z4 macrosatellite. *Nucleic Acids Res.* **47**, 2822–2839 (2019).
- A. V. Gendrel *et al.*, Epigenetic functions of smcHD1 repress gene clusters on the inactive X chromosome and on autosomes. *Mol. Cell. Biol.* **33**, 3150–3165 (2013).
- N. Jansz, K. Chen, J. M. Murphy, M. E. Blewitt, The epigenetic regulator SMCHD1 in development and disease. *Trends Genet.* **33**, 233–243 (2017).
- K. Chen *et al.*, Genome-wide binding and mechanistic analyses of SmcHD1-mediated epigenetic regulation. *Proc. Natl. Acad. Sci. U.S.A.* **112**, E3535–E3544 (2015).
- Y. Wang *et al.*, ZNF280A promotes proliferation and tumorigenicity via inactivating the hippo-signaling pathway in colorectal cancer. *Mol. Ther. Oncolytics* **12**, 204–213 (2019).
- H. Liu, Y. Qin, N. Zhou, D. Ma, Y. Wang, ZNF280A promotes lung adenocarcinoma development by regulating the expression of EIF3C. *Cell Death Dis.* **12**, 39 (2021).
- S. Gao, C. L. Hsieh, J. Zhou, L. Shemshedin, Zinc finger 280B regulates sGC α 1 and p53 in prostate cancer cells. *PLoS One* **8**, e78766 (2013).
- J. Zhai *et al.*, ZNF280B promotes the growth of gastric cancer *in vitro* and *in vivo*. *Oncol. Lett.* **15**, 5819–5824 (2018).
- P. Caron, J. van der Linden, H. van Attikum, Bon voyage: A transcriptional journey around DNA breaks. *DNA Repair (Amst.)* **82**, 102686 (2019).
- K. Hilmi *et al.*, CTCF facilitates DNA double-strand break repair by enhancing homologous recombination repair. *Sci. Adv.* **3**, e1601898 (2017).
- F. Lang *et al.*, CTCF prevents genomic instability by promoting homologous recombination-directed DNA double-strand break repair. *Proc. Natl. Acad. Sci. U.S.A.* **114**, 10912–10917 (2017).
- Y. Ying *et al.*, Oncogenic HOXB8 is driven by MYC-regulated super-enhancer and potentiates colorectal cancer invasiveness via BACH1. *Oncogene* **39**, 1004–1017 (2020).
- T. Liu *et al.*, Cistrome: An integrative platform for transcriptional regulation studies. *Genome Biol.* **12**, R83 (2011).
- J. Ernst, M. Kellis, ChromHMM: Automating chromatin-state discovery and characterization. *Nat. Methods* **9**, 215–216 (2012).
- Z. Chen, M. N. Djekidel, Y. Zhang, Distinct dynamics and functions of H2AK119ub1 and H3K27me3 in mouse preimplantation embryos. *Nat. Genet.* **53**, 551–563 (2021).
- J. Zhang *et al.*, Targeted inhibition of KDM6 histone demethylases eradicates tumor-initiating cells via enhancer reprogramming in colorectal cancer. *Theranostics* **10**, 10016–10030 (2020).
- A. Subramanian *et al.*, Gene set enrichment analysis: A knowledge-based approach for interpreting genome-wide expression profiles. *Proc. Natl. Acad. Sci. U.S.A.* **102**, 15545–15550 (2005).
- B. G. Wilson *et al.*, Epigenetic antagonism between polycomb and SWI/SNF complexes during oncogenic transformation. *Cancer Cell* **18**, 316–328 (2010).
- X. S. Shu *et al.*, The epigenetic modifier PBRM1 restricts the basal activity of the innate immune system by repressing retinoic acid-inducible gene-I-like receptor signalling and is a potential prognostic biomarker for colon cancer. *J. Pathol.* **244**, 36–48 (2018).
- Cancer Genome Atlas Network, Comprehensive molecular characterization of human colon and rectal cancer. *Nature* **487**, 330–337 (2012).
- L. Marisa *et al.*, Gene expression classification of colon cancer into molecular subtypes: Characterization, validation, and prognostic value. *PLoS Med.* **10**, e1001453 (2013).
- J. Sabates-Bellver *et al.*, Transcriptome profile of human colorectal adenomas. *Mol. Cancer Res.* **5**, 1263–1275 (2007).